Supplement of Atmos. Chem. Phys., 22, 15943–15962, 2022
https://doi.org/10.5194/acp-22-15943-2022-supplement

Atmospheric Chemistry and Physics
Open Access

Supplement of

Aerosol activation characteristics and prediction at the central European ACTRIS research station of Melpitz, Germany

Yuan Wang et al.

Correspondence to: Yuan Wang (wang_yuan@lzu.edu.cn) and Silvia Henning (henning@tropos.de)

Text S1. Relationship between aerosol hygroscopicity factor calculated from the chemical composition and the individual composition groups.

For understanding the relationship between aerosol hygroscopicity factor calculated from the chemical composition (κ_{chem}) and the individual composition groups, it is important to realize that these groups do not act in the same way in Eq 3. The influence of organics is direct. As shown in Table 1, the hygroscopicity of organics (κ_{org}) is smaller than that of inorganics (κ_{inorg}). Thus, higher mass fraction of organics (f_{org}) means lower κ_{chem}, as shown in Figure S5a. But with SO_4, NH_4, NO_3 it is more complicated because they are coupled through the ion balance. As shown in Figure 5c, the absolute amount of SO_4 and NH_4 seems stable, but the NO_3 amount changes a lot between the seasons. The presence of NO_3 shifts the salts from mostly $(NH_4)_2SO_4$ towards NH_4NO_3 and NH_4HSO_4 or even H_2SO_4. Hygroscopicity factors (κ) are very similar between $(NH_4)_2SO_4$, NH_4HSO_4, and NH_4NO_3, but κ of H_2SO_4 is much higher. Thus, an increase in NO_3 can have a dual impact on κ for this data set, causing the positive correlation between mass fraction of nitrate and κ_{chem} in Figure S5b. The increase in NO_3 adds a higher proportion of salt and increases the κ of SO_4. So, if mass fraction of SO_4 ($f_{sulfate}$) decreases because more organics is present, κ decreases. If $f_{sulfate}$ decreases because more NO_3 is present, k increase. As these two trends are opposite, the correlation of $f_{sulfate}$ and κ_{chem} will be poor.

Text S2. Yearly variations of CCN activation characteristics.

Yearly trends of CCN activation properties are investigated. The CCN number concentration (N_{CCN}) and hygroscopicity factor calculated from monodisperse CCN measurements (κ_{CCN}) measured at supersaturation (*SS*) of 0.1% and 0.7% are chosen to represent the CCN activation characteristics. The results are shown in Figure S7. The yearly trends in N_{CCN} and κ_{CCN} are not significant (without significant increase or decrease trends) during the measurements from August 2012 to October 2016. However, it is interesting to see that the N_{CCN} measured in 2015 was significantly lower than it measured in other four years. One of the reasons could be that the CCN measurements in 2015 concentrated in summer and autumn, lacking measurements in the spring and winter months (Figure S1). As shown in Figure 3b, N_{CCN} measured at summer and autumn are lower than those measured in spring and winter due to its seasonal trend, causing the lowest median N_{CCN} values in 2015. Thus, the CCN measurements in 2015 may not be representative of the CCN characteristics of the whole year. Similarly, the 2012 measurements may not be representative of year-round CCN characteristics because of the lacking spring and summer measurements. Additionally, it is also hard to see the yearly trends of CCN activation characteristics using the only 4-year data. In order to investigate the yearly trends of CCN activation characteristics, longer-term measurements are required.

Text S3. Method for evaluating the impact of N_{CCN} overestimation on cloud radiative forcing and autoconversion process

Cloud optical thickness (τ) can be expressed by (Stephens, 1984)

$$\tau \approx \frac{3}{2} W r_e^{-1}, \tag{1}$$

where W is the liquid water path, r_e is the effective radius of cloud droplets. Meanwhile r_e is proportional to the volume weighted mean radius of cloud droplets (r_v) (Bower and Choularton, 1992) and can be expressed by

$$r_e = \beta \left(\frac{3q}{4\pi\rho_w N_c}\right)^{1/3} = \beta r_v, \tag{2}$$

where β is the scaling factor, q is the cloud liquid water content, ρ_w is the density of water, and N_c is the number concentration of cloud droplet. Here, to focus on the effect of N_c on r_e, β is specified as a fixed parameter, i.e., ignoring the dispersion effect, as assumed in many climate models (Quaas et al., 2004).

According to Liu et al. (2004, 2005), parameterization of the autoconversion process can be expressed by

$$P = TA \times P_0, \tag{3}$$

where P is the autoconversion rate, P_0 is the rate function describing the conversion rate after the onset of the autoconversion process, and TA is a function describing the threshold behavior of the autoconversion process. Meanwhile, TA can be expressed by

$$TA = \left[\frac{\int_{r_c}^{\infty} r^6 n(r) dr}{\int_0^{\infty} r^6 n(r) dr}\right]\left[\frac{\int_{r_c}^{\infty} r^3 n(r) dr}{\int_0^{\infty} r^3 n(r) dr}\right], \tag{4}$$

where r is the droplet radius, $n(r)$ is the cloud droplet size distribution, and r_c is the critical radius of autoconversion process. The *TA* ranges from zero to one, with a larger *TA* indicating a greater probability that the collision process occurs in clouds. Liu et al. (2006) derived the analytical expression of r_c as follows:

$$r_c \approx 4.09 \times 10^{-4} \beta_{con}^{1/6} \frac{N_c^{1/6}}{q^{1/3}}, \tag{5}$$

where $\beta_{con} = 1.15 \times 10^{23}$ s^{-1} is an empirical constant.

Essentially, an overestimation of N_{CCN} leads to overestimate N_c in models. From the 3rd and 4th scheme to 5th scheme, the slope of the linear fitting decreases 0.1 on average, meaning that the ~10% overestimation of N_{CCN} and N_c is reduced. According to equations 1 and 2, it can reduce 3.1% underestimation of r_e when assuming the constant q and β, thereby reducing 3.2% overestimation of τ. When assuming the global average cloud shortwave cooling effect is 40 Wm^{-2} (Lee et al., 1997), the corresponding difference is 1.28 Wm^{-2}, which amounts to 32% of the direct radiative forcing from a doubling CO_2 (about 4 Wm^{-2}). Additionally, according to the equations 4 and 5, it can reduce the overestimation of r_c thus the underestimation of *TA*, indicating that the underestimation of the strength of autoconversion process can be reduced.

Text S4. N_{CCN} predictions using the seasonally mean value of κ over D_p of 100 to 200 nm

The main size dependence of κ occurs at D_p of ~40 to 100 nm as shown in Figure 6a, which would be for *SS* larger than 0.2%. At D_p of 100 to 200 nm corresponding to *SS* less than 0.2%, κ almost stays constant. The mean value of κ at D_p of 100 to 200 nm is close to 0.3 for spring and winter, and that's where deviations in Figure S7c are small. However, the mean value of κ at D_p of 100 to 200 nm overestimates the κ for *SS* larger than 0.2% at each season. We further compare the N_{CCN} predictions between using the seasonally mean value of κ over D_p of 100 to 200 nm and the κ - D_p power-law fit. As shown in Figure S8, at *SS* = 0.1 and 0.2%, the seasonally mean κ value over D_p of 100 to 200 nm and κ - D_p power-law fit both predict the N_{CCN} well at each season, while the mean κ value over D_p of 100 to 200 nm leads to a significant overestimation of N_{CCN} within 10% on average at *SS* = 0.3, 0.5, and 0.7%. Therefore, to predict the N_{CCN} at a relatively low *SS* of less than 0.2% (e.g., in fog and shallow stratiform cloud), the mean κ value over D_p of 100 to 200 nm also works well.

Reference

Bower, K. N., and Choularton, T. W.: A parameterization of the effective radius of ice-free clouds for use in global climate models, Atmos. Res., 27, 305– 339, 1992.

Eichler, H., Cheng, Y. F., Birmili, W., Nowak, A., Wiedensohler, A., Brüggemann, E., Gnauk, T., Herrmann, H., Althausen, D., Ansmann, A., Engelmann, R., Tesche, M., Wendisch, M., Zhang, Y. H., Hu, M., Liu, S., and Zeng, L. M.: Hygroscopic properties and extinction of aerosol particles at ambient relative humidity in South-Eastern China, Atmos. Environ., 42, 6321–6334, https://doi.org/10.1016/j.atmosenv.2008.05.007, 2008.

Fors, E. O., Swietlicki, E., Svenningsson, B., Kristensson, A., Frank, G. P., and Sporre, M.: Hygroscopic properties of the ambient aerosol in southern Sweden – a two year study, Atmos. Chem. Phys., 11, 8343–8361, https://doi.org/10.5194/acp-11-8343-2011, 2011.

Lee, W., Iacobellis, S. F., & Somerville, R. C. J.: Cloud Radiation Forcings and Feedbacks: General Circulation Model Tests and Observational Validation, Journal of Climate, 10(10), 2479-2496, 1997.

Liu, Y., Daum, P. H., and McGraw, R.: An analytical expression for predicting the critical radius in the autoconversion parameterization, Geophys. Res. Lett., 31(6), L06121, 2004.

Liu, Y., Daum, P. H., and McGraw, R.: Size truncation effect, threshold behavior, and a new type of autoconversion parameterization, Geophys. Res. Lett., 32(11), L11811, 2005.

Liu, Y., Daum, P. H., McGraw, R., and Miller, M.: Generalized threshold function accounting for effect of relative dispersion on threshold behavior of autoconversion process, Geophys. Res. Lett., 33(11), L11804, 2006.

Quaas, J., Boucher, O., and Breon, F. M.: Aerosol indirect effects in POLDER satellite data and the Laboratoire de Meteorologie Dynamique Zoom (LMDZ) general circulation model, J. Geophys. Res., 109, 2004.

Stephens, G. L.: The parameterization of radiation for numerical weather predication and climate models, Mon. Weather Rev., 112, 826–867, 1984.

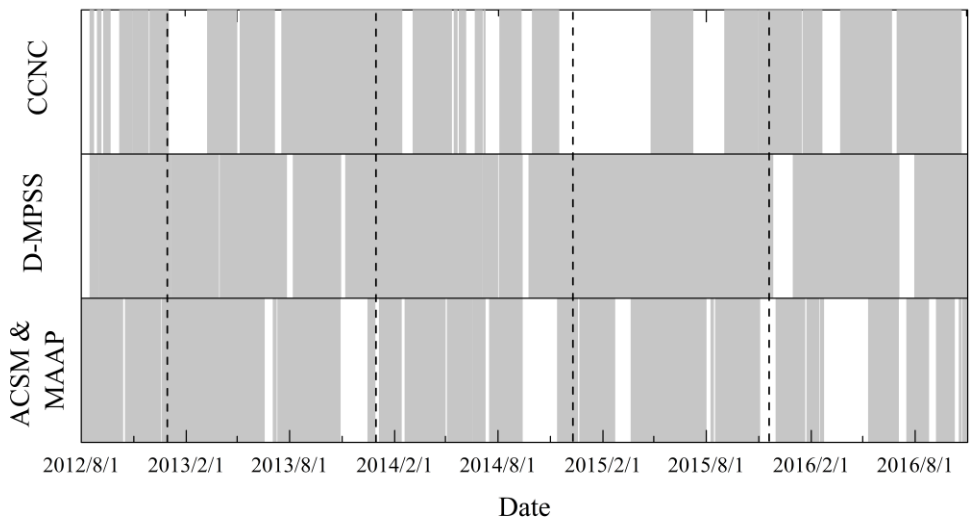

Figure S1. Coverage of the effective data represented by the gray columns during the long-term experiment at Melpitz. CCNC — cloud condensation nuclei counter, D-MPSS — Dual-mobility particle size spectrometer, ACSM — aerosol chemical species monitor, MAAP — multi-angle absorption photometer.

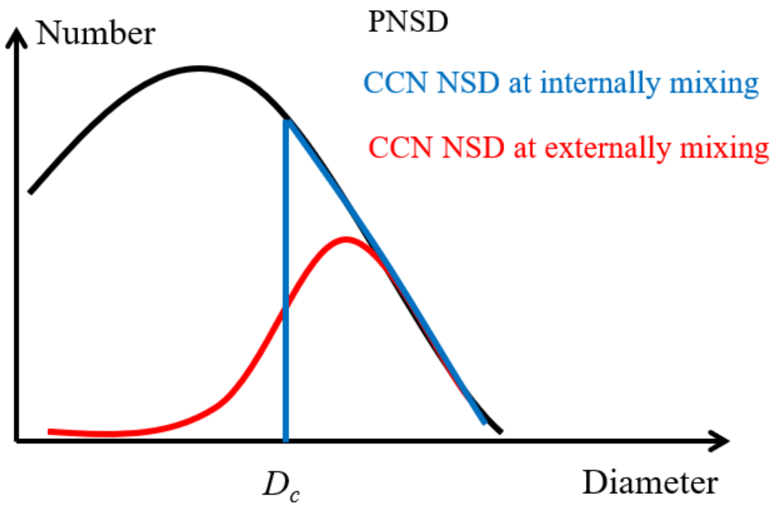

Figure S2. Schematic diagram for the relationship among the particle number size distribution (PNSD), CCN number size distribution (CCN NSD) at internally mixing, and the CCN NSD at externally mixing.

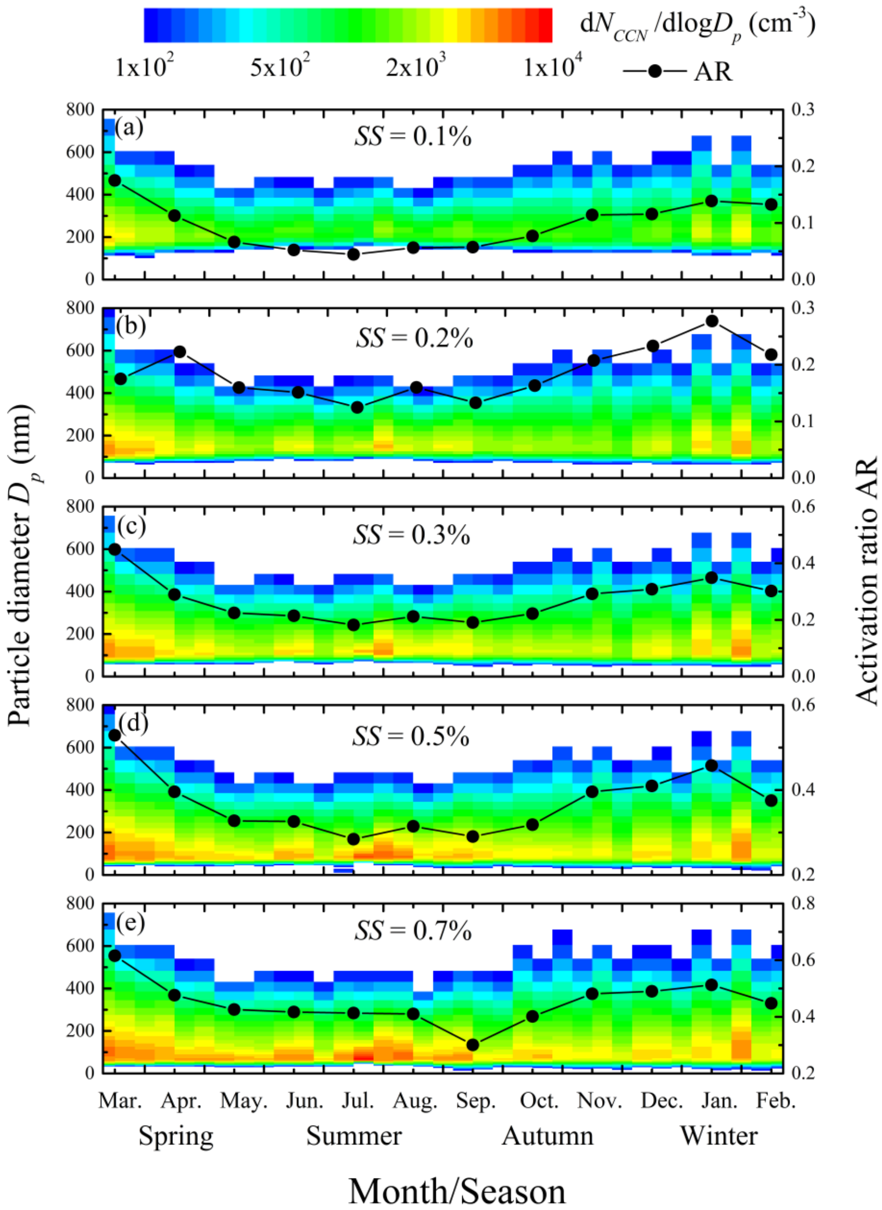

Figure S3. Monthly variations of CCN number size distributions and activation ratios (AR) at five different supersaturation (*SS*) conditions. The CCN number size distribution was the result of using an average of every ten days. The black dot presents the median AR at each month.

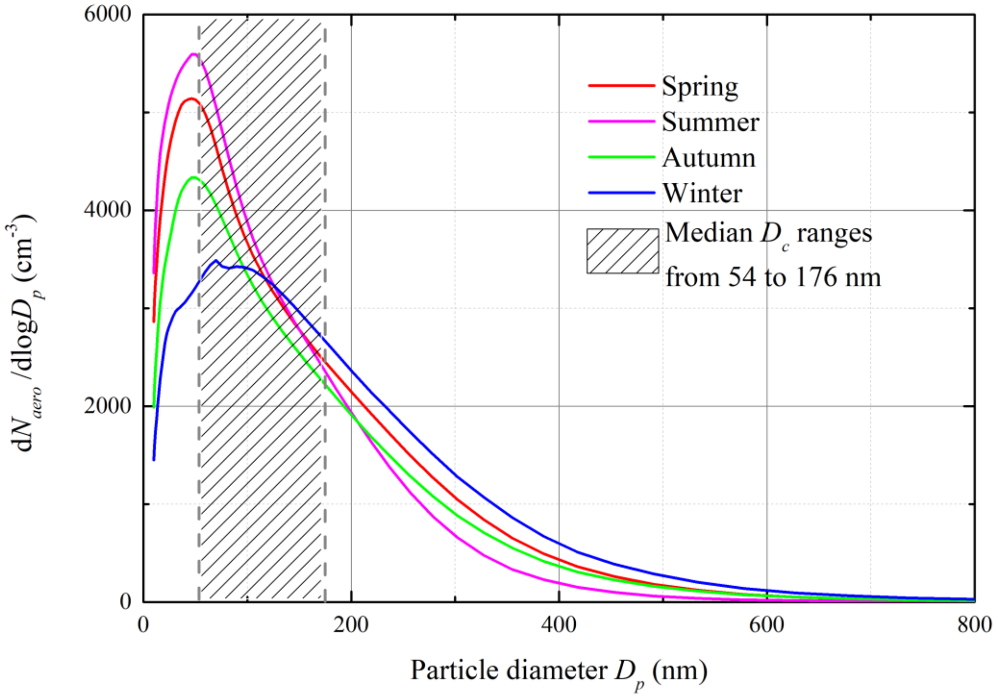

Figure S4. Mean particle number size distribution at each season.

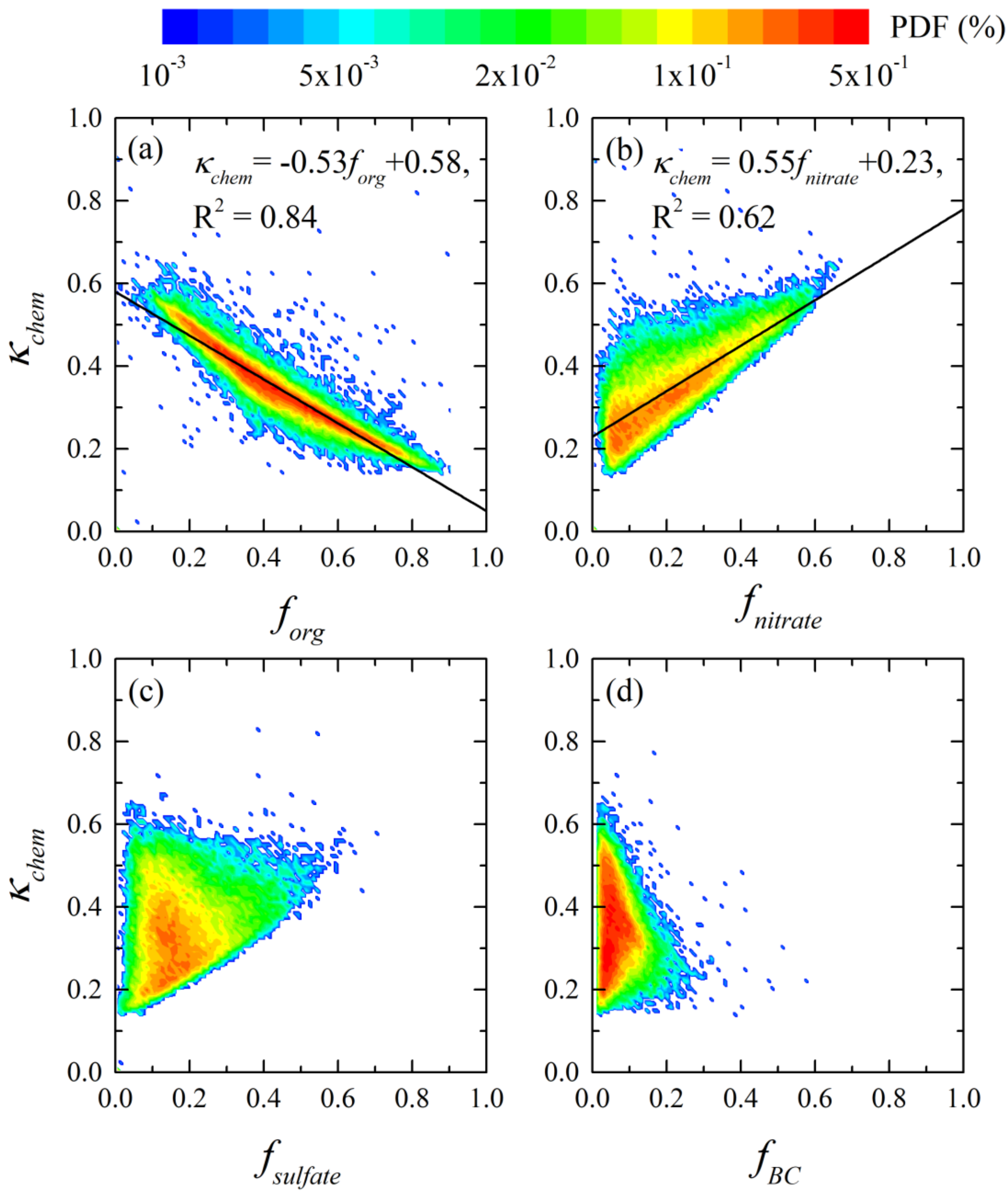

Figure S5. Relationships between (a) aerosol hygroscopicity factor calculated from the chemical composition (κ_{chem}) and mass fraction of organics (f_{org}) in submicron aerosol, (b) κ_{chem} vs. mass fraction of nitrate ($f_{nitrate}$), (c) κ_{chem} vs. mass fraction of nitrate ($f_{sulfate}$), and (d) κ_{chem} vs. mass fraction of black carbon (f_{BC}). Color bar represents the probability density function (PDF). Black lines are linear fit lines.

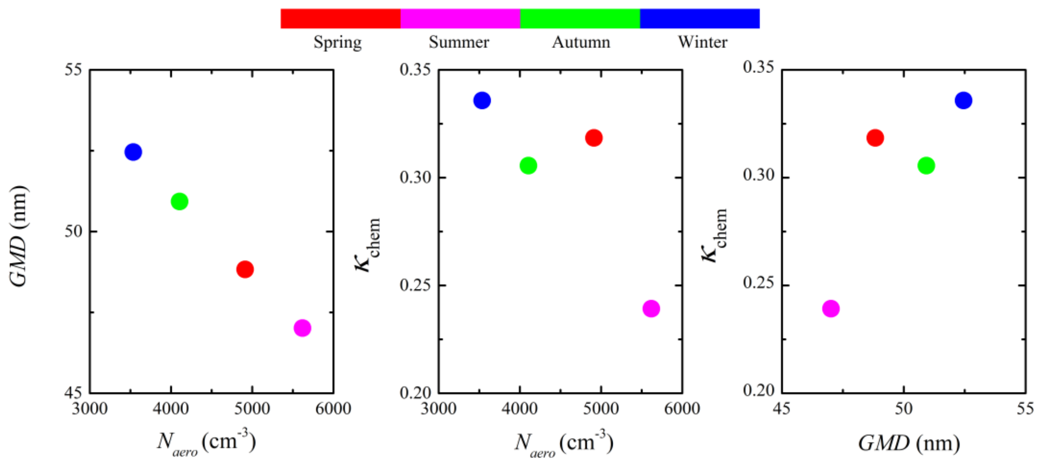

Figure S6. Relationships among seasonal median values of aerosol number concentration with diameter raging 10 to 800 nm (N_{aero}), geometric mean diameter of aerosol particles (*GMD*), and particle hygroscopicity parameter calculated from the chemical compositions (κ_{chem}). The dots represent the median values at each season.

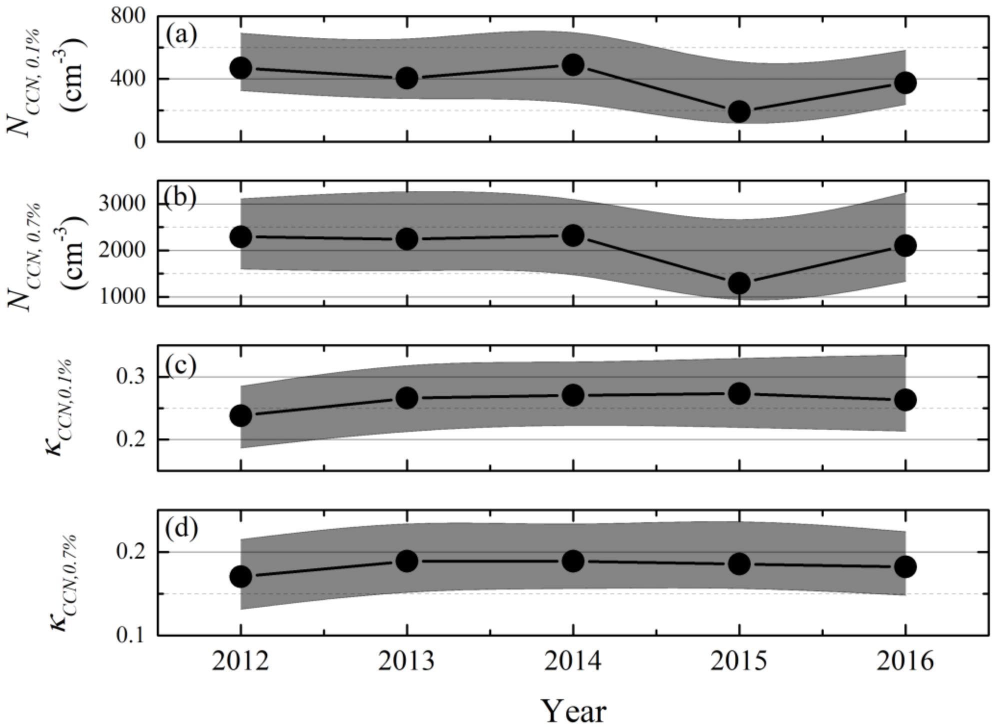

Figure S7. Yearly variations of (a) CCN number concentration (N_{CCN}) at supersaturation (*SS*) of 0.1% ($N_{CCN,0.1\%}$), (b) N_{CCN} at *SS* of 0.7% ($N_{CCN,0.7\%}$), (c) hygroscopicity factor calculated from monodisperse CCN measurements (κ_{CCN}) at *SS* of 0.1% ($\kappa_{\mathrm{CCN,\ 0.1\%}}$), and (d) κ_{CCN} at *SS* of 0.7% ($\kappa_{\mathrm{CCN,\ 0.7\%}}$). Dots represent the median values. Shaded areas represent the values in the range from 25$^{\mathrm{th}}$ to 75$^{\mathrm{th}}$ percent.

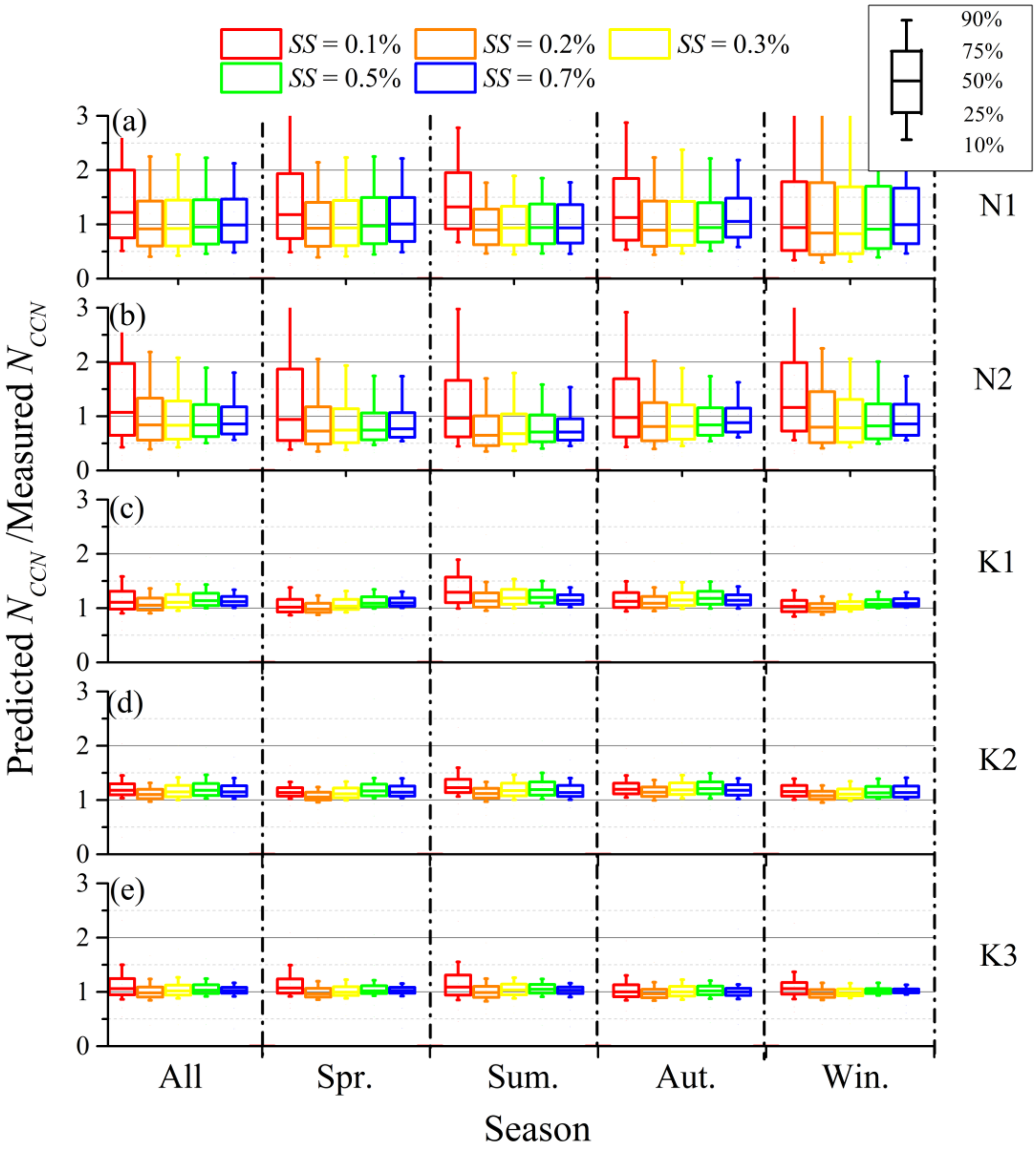

Figure S8. Statistics of the ratio of predicted CCN number concentration (N_{CCN}) to the measured one at different supersaturation (*SS*) conditions for each season and all datasets. The (a), (b), (c), (d), and (e) represent the prediction results from the N1, N2, K1, K2, and K3 scheme, respectively. Introduction for the schemes is in Table 3.

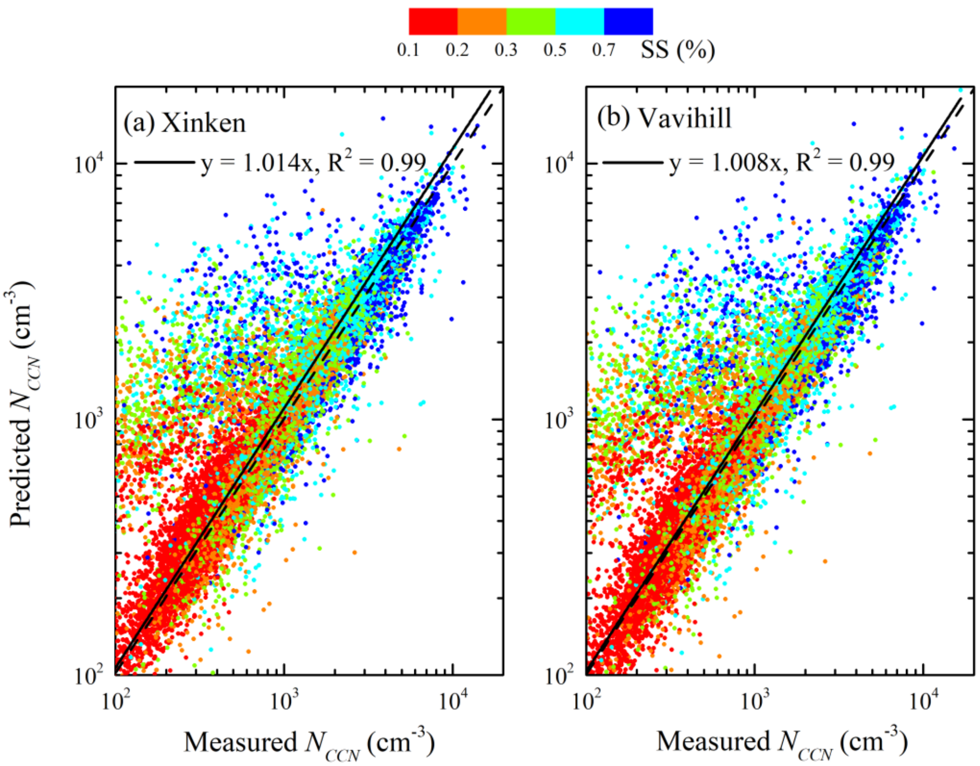

Figure S9. Predicted vs. measured CCN number concentration (N_{CCN}) at Melpitz. (a) using the κ - D_p power-law fitting measured at Xinken station in China (Eichler et al., 2008) to predict the Melpitz N_{CCN}; (b) using the κ - D_p power-law fitting measured at Vavihill station in Sweden (Fors et al., 2011). Dashed line is the 1:1 line and solid line is the linear fitting.

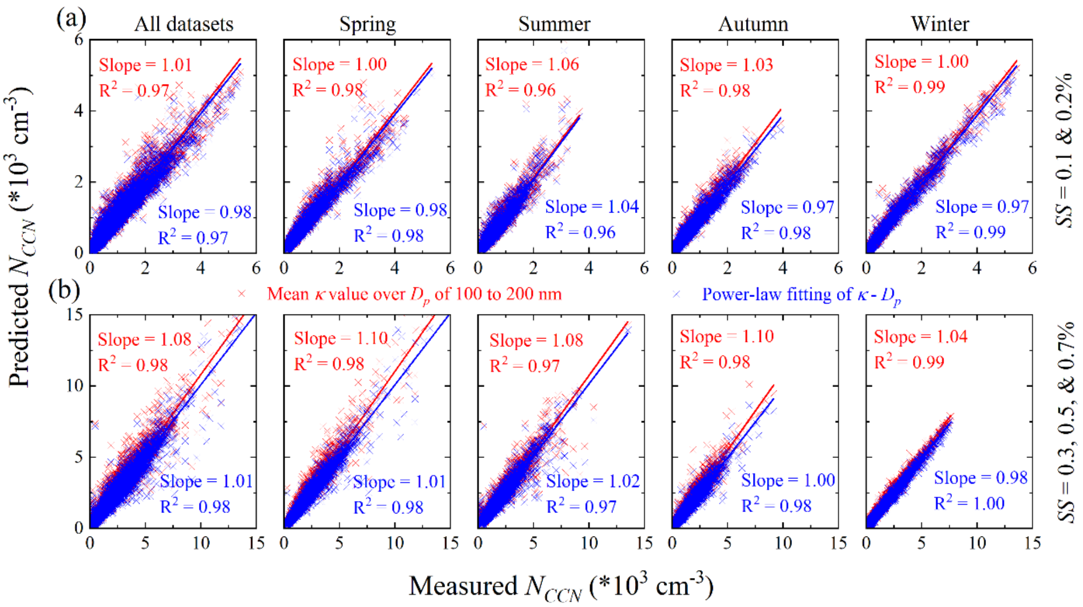

Figure S10. Predicted vs. measured CCN number concentration (N_{CCN}) at different supersaturation (*SS*) conditions for different seasons. (a) results at *SS* = 0.1 and 0.2%; (b) results at *SS* = 0.3, 0.5, and 0.7%. Red cross represents the predicted N_{CCN} using mean hygroscopicity factor (κ) over particle diameter (D_p) of 100 to 200 nm, while the blue cross represents the predicted N_{CCN} using power-law fit of κ and D_p. Red and blue lines are the linear fits.

Table S1. Summary of CCN number concentration (N_{CCN}) at different supersaturation (SS) conditions measured at different locations (data for Figure 2).

Location (coordinates; a.m.s.l)	Type	Period	SS (%)	Mean N_{CCN} (cm^{-3})	Reference
Melpitz, Germany (51.5°N, 12.9°E; 86 m)	rural, continental	Aug. 2012–Oct. 2016	0.1 0.2 0.3 0.5 0.7	513 1102 1466 2020 2477	Present study
Vavihill, Sweden (56.0°N, 13.2 °E; 172 m)	rural	May 2008–Jul 2010	0.1–1.0	362–1795	Fors et al., 2011
Southern Great Plains, USA (36.6°N, 97.5°W; 320 m)	rural, agricultural	Sep. 2006–Apr. 2011	0.4	1248	Liu and Li, 2014
Hyytiälä, Finland (61.9°N, 24.3°E; 181 m)	rural	Feb. 2009–Dec. 2012	0.1–1.0	274–1128	Paramonov et al., 2015
Mahabaleshwar, India (17.9°N, 73.7°E; ~490 m)	rural	Jun. 2015	0.1–0.94	118–1826	Singla et al., 2017
Guangzhou, China (23.6°N, 113.1°E; ~21 m)	rural	Jul. 2006	0.068–0.67	995–10731	Rose et al., 2010
Wuqing, China (39.4°N, 117.0°E; 7.4 m)	suburban	Dec. 2009–Jan. 2010	0.056–0.7	2192–12963	Deng et al., 2011
Seoul, Korea (37.6°N, 127.0°E; ~38 m)	urban	2004–2010	0.4–0.8	4145–6067	Kim et al., 2014
Mahabubnagar, India (17.7°N, 78.9°E; ~490 m)	polluted continental	Oct. 2011	1.0	~5400	Varghese et al., 2016

Table S2. Error function fits for the relationships between activation ratio (AR) vs. supersaturation (*SS*), and CCN number concentration (N_{CCN}) vs. *SS* for different seasons. The equation is y=a+a*erf(ln(x/b)/c), where a, b, and c are parameters remained to be determined. The a_{AR} and a_{NCCN} represent the parameter a in AR vs. *SS* fitting and N_{CCN} vs. *SS* fitting, respectively.

Season	a_{AR}	a_{NCCN}	*b*	*c*	R^2
Spring	0.50	2637	0.72	2.33	0.998
Summer	0.51	3162	1.04	2.15	0.997
Autumn	0.56	2443	0.84	2.29	0.999
Winter	0.44	1624	0.29	1.83	0.999
All	0.40	2199	0.59	2.25	0.998